Chapter 3

Dynamic Modelling of Rolling Element Bearing

For assessing fault severity of components of bearing upon rotor-bearing system, a non-linear dynamic vibration model using six degrees of freedom is developed in this chapter. The severity assessment is based upon varying defect sizes of outer and inner race, which are introduced in model. The equation of motion obtained from model were solved and simulated to obtain vibration responses due to defects. Experiments are carried out with rotor-bearing system and analyzed using continuous wavelet transform (CWT). CWT technique provides time interval between two consecutive amplitudes corresponds to fault frequencies. The CWT results are very useful for determining the presence of fault under its various degrees of severity.

3.1. Introduction

In rotating machinery, most critical and important component is rolling element bearing. The operational behavior of the rolling element bearing governs the performance of rotating machinery. The presence of fault in rolling element bearing initiates high level of vibration into the system. This leads to various damage and anomalies into rotary system, resulting into loss of production due to damage in the bearing. Early detection of fault, is the reliable and potential source of preventing the rolling element bearing from large damage. However, after certain degree of the damage reached, rolling element bearing should be replaced. But, in order to understand the replacement time of damaged bearing, it is highly important to understand the severity of fault occurred in rolling element bearing. Therefore, in this chapter, severity of fault assessment is carried out with the help of mathematical modelling as well as experimental analysis. Vibration monitoring of bearing has been widely used to monitor and detect the presence of fault with the help of dominant fundamental defect frequencies. But the dominant peak of defect is non-stationary in nature, which is difficult to understand and gain information about the defect, with the help of conventionally used signal processing technique such as time and frequency domain. Hence, the noisy vibration signal obtained from the defective rolling element bearing,

needs to be processed using advanced signal processing techniques like Hilbert – Haung transform (HHT), Short time fourier transform (STFT), Wavelet transform (WT) etc., in order to obtain the exact faulty features of the bearing. Therefore, this study describes some of the potential contribution by various researchers in the field of fault diagnosis of rolling element bearing using mathematical modelling and advanced signal processing technique. Sassi et.al [1] developed a new application called bearing toolbox for simulating the vibratory response of bearings to obtain excitations produced by the local defect. Sopanen and mikkola [2-3], developed a dynamic model of deep-groove ball bearing to understand the effect of diametric clearance between the rolling element and raceway upon the level of vibration and on the natural frequencies. Tadina et.al [4] developed an improved comprehensive model to obtain vibration response due to faults during run-up. In their model, they considered the effect of centrifugal load and radial clearance and the balls contact force is described by a non-linear Hertzian contact deformation. Petersen et.al [5] developed the model for a radially loaded double row bearing of varying stiffness with a raceway defect of varying size of depth, length and surface roughness. The model is developed to calculate and analyze quasi-static load distribution. Ahmadi et.al [6] proposed a dynamic model which takes the finite rolling element size in consideration. A similar analytical model has been proposed by Kiral and Karagulle [7] for predicting the vibration response due to the local defect. They modelled the outer race and its housing using the finite elements and applied radially distributed load for each node, in order to obtain amplified local defect. Antoni et.al [8] proposed a technique of modulation intensity distribution for estimating the size of bearing fault.

Vibration response signals obtained from defective rolling element bearing are non-stationary in nature [9]. Application of simple signal processing techniques like time domain analysis and frequency domain analysis upon such a noisy and non-stationary signal, merely provide any information about the presence of defect. Hence such a signal needs to be processed using advanced signal processing techniques. Over the years many advancements have been observed, in advanced signal processing techniques and many researchers used these techniques for the fault diagnosis of rolling element bearing subjected to various fault conditions. Sawalhi and Randall [10], used the method of

spectrum kurtosis (SK) and minimum entropy deconvolution (MED) for analyzing the noisy vibration response signals of bearing faults. The results described that double impact phenomenon ascribed to fault signals of the outer raceway of the bearing after denoising the signal. Randall and Swalhi [11] also used the minimum entropy deconvolution method for obtaining the information about the defect size, by separating the impulses from entry event into and exit event process from an individual fault. Hong and Liang [12] proposed the method for bearing fault severity measurement based on the Lempel-Ziv complexity and continuous wavelet transform. Their result indicated that Lempel-Ziv complexity was found to be proportional for outer race defects and inversely proportional for inner race defects to fault severity (fault size) for all rotational speed.

However, severity of faults of components of the bearing still needs to be comprehensively analyzed, mathematically and experimentally. The contribution of this research is to test the feasibility of continuous wavelet transform for understanding the effect of fault severity of outer race, inner race and rolling element, upon the rotor-dynamic system.

In this chapter, study is divided into parts, in order to analyze the defective rolling element bearing. First part of the study develops the non-linear mathematical modelling of rolling element bearing with 6-degrees of the freedom, including the modelling of outer race defect, inner race defect and ball defect.

The second part of the study validates simulated vibration response with the experimental analysis, where simulated and experimental vibration response are validated and presented for time domain, frequency domain and time-frequency domain (CWT). Here, baseline data assessment is conducted for both simulation and experimentation, using healthy bearing, in order to differentiate the vibration response caused by the varying compliance and local defect.

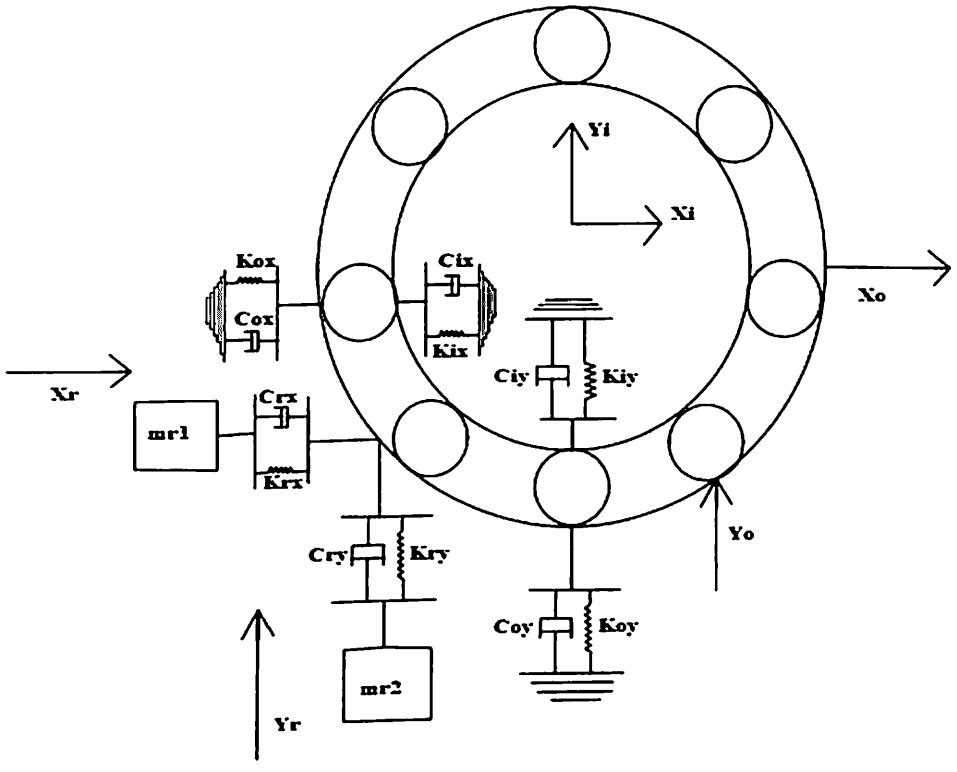

Figure 3.1 Six-DOF dynamic model of Bearing

3.2. Dynamic Modelling of the bearing

A non-linear Vibration model of bearing with 6-DOF (degrees of freedom) is proposed in this paper as shown in Figure 3.1, to obtain the vibration response of the bearing due to the localized defect. The model mainly consists of 4-DOF in the horizontal and vertical directions of inner race and outer race and 2 DOF unit resonators are used in horizontal as well vertical direction. The function of unit resonators is to compensate high-frequency resonant response of bearing due to defects upon the surface of bearing components, by adjusting its stiffness and damping co-efficient. The mass-spring-damper system was attached in both the directions to the outer raceway in order to predict high-frequency resonant response in both the radial directions. The static load 'W' is applied to the inner raceway, to obtain the vibration response in the radially loaded condition of bearing. The model was based upon the following assumptions:

1. The motions of the rolling elements, inner and outer races and the rotor are in the plane of the bearing only.
2. Mass of each component of bearing is considered to be lumped.

3. Moment of inertia and centrifugal load of each component is ignored.

4. Slippage of the balls during rolling on the surface of the races is not present.

5. Forces are acting in the radial directions only along X and Y directions.

6.The effect of the surface waviness and other geometric errors are ignored and assumed that only the localized defect is present.

7.Contact deformation between the rolling element and raceway is considered according to Hertzian theory of elasticity.

8.Damping due to the Elasto-hydrodynamic lubrication (EHL) is considered and all damping is considered to be linearly viscous.

Non-linear dynamic differential equation of the bearing is as shown below:

$$m_i\ddot{x}_i + c_i\dot{x}_i + k_i x_i + f_x = 0$$

$$m_i\ddot{y}_i + c_i\dot{y}_i + k_i y_i + f_y = Ft$$

$$m_o\ddot{x}_o + (c_{ox} + c_{rx})\dot{x}_o + (k_{ox} + k_{rx})x_o - k_{rx}x_r - c_{rx}\dot{x}_r - f_x = 0 \qquad (3.1)$$

$$m_o\ddot{y}_o + (c_{oy} + c_{ry})\dot{y}_P + (k_{oy} + k_{ry})y_o - k_{ry}y_r - c_{ry}\dot{y}_r - f_y = 0$$

$$m_{r1}\ddot{x}_r + C_{rx}(\dot{x}_r - \dot{x}_o) + k_{rx}(x_r - x_o) = 0$$

$$m_{r2}\ddot{y}_r + C_{ry}(\dot{y}_r - \dot{y}_o) + k_{ry}(y_r - y_o) = 0$$

Where m_i represents the mass of inner raceway and shaft , m_o represents mass of outer raceway and bearing support structure and m_{r1} and m_{r2} represents mass of unit resonators in radial horizontal and vertical directions. The six degrees of the freedom included in the model are represented by x_i and y_i for the inner raceway displacement, x_o and y_o for the outer raceway displacement and the measured vibration response is represented by x_r and y_r. k_i, k_o and k_r represents the stiffness of the inner raceway, outer raceway and unit resonator in the horizontal and vertical direction. c_i, c_o and c_r represents damping of inner raceway, outer raceway and unit resonator in the horizontal and vertical direction. The vibration response is non-linear vibration due to the non-linearity of stiffness. The stiffness and damping co-efficient are adjusted to describe the low-frequency mode of the bearing-structure. f_x & f_y are non-linear contact force of the bearing in the vertical and horizontal

direction. 'Ft' represents the applied radial load upon the inner raceway in vertical direction.

Equation (3.1) is non-linear, coupled and ordinary differential equation which is solved by using Runge-Kutta method and ode45 solver is used in MATLAB to solve the non-linear equation.

3.2.1 Kinematics of the rolling elements including slippage

The main fundamental components of the bearing are the outer race, the inner race, the cage and the rolling element. Important parameters of the bearing are the bearing pitch diameter D_p , rolling element diameter D_b , number of balls n_b and contact angle α . The shaft rotates at the rotating angular speed of $\omega_s = 2\pi f_s$, where f_s is the shaft rotating frequency. The resulting nominal cage speed $\omega_c = 2\pi f_c$ is given by

$$\omega_c = \frac{\omega_s}{2}\left(1 - \frac{D_b \cos\alpha}{D_p}\right) \tag{3.2}$$

The angular position ϕ_j of the j^{th} rolling element without slippage is given by

$$\phi_j = \phi_o + 2\pi(j-1)/N_b + \omega_c\, dt \tag{3.3}$$

The effect of the slippage on the angular position ϕ_j of the j^{th} rolling element is given by

$$\phi_j = \phi_o + 2\pi(j-1)/N_b + \omega_c\, dt + (0.5 - rand) \times \phi_{slip} \tag{3.4}$$

where $j = 1\ to\ N_b$, ϕ_o is the initial angular position of bearing cage.

The slippage defined in equation (4) is dependent upon the phase deviation ϕ_{slip} . The relation between the frequency deviation and the phase deviation is given by

$$\Delta f = \phi_{slip} f_m \tag{3.5}$$

where Δf is the maximum frequency deviation (Hz), f_m is the modulation frequency (Hz) and ϕ_{slip} is the maximum phase deviation (rad).

Slippage in the rolling element bearing is defined in terms of the percentage variation of the mean frequency of impact which is given as

$$\phi_{slip} = \frac{\Delta f}{f_m} \times 100\% \tag{3.6}$$

The usual range of the slippage in rolling element bearing is in between 1%-2% and this corresponds to the phase variation (ϕ_{slip}) of (0.01-0.02 rad). In this paper, the effect of the slippage is taken into consideration during computation of equation of motion.

3.2.2 Contact deformation of the bearing without defect

The contact deformation δ_j of rolling element j is the functions of the relative displacements of the inner raceway$(x_i - x_0)$ and outer raceway$(y_i - y_0)$, the position of the rolling element ϕ_j and the internal radial clearance C_r is given by

$$\delta_j = (x_i - x_0)cos\phi_j + (y_i - y_0)sin\phi_j - C \tag{3.7}$$

According to the Hertz contact theory of deformation, the non-linear contact force f is associated with the contact deformation δ_j and is given by

$$f = K\delta_j^n \tag{3.8}$$

where K is the time-varying non-linear contact stiffness,n is the load-deflection parameter equals to 3/2 for ball bearing and 10/9 for roller bearing [13]
The non-linear contact stiffness depends upon the radius of the curvature of the raceways and material properties of the surfaces in contact, as well upon the load deflection parameter. The curvature is given by

$$\rho = \frac{1}{r} \tag{3.9}$$

r denotes the radius of curvature. As per the sign convention followed, curvature may be positive or negative, positive radius denotes the convex surfaces and negative radius denotes the concave surfaces. For the two contacting steel bodies of different radius of curvature, the relative approaches between the rolling element and each raceway is given by

$$\delta = \delta_i + \delta_o \tag{3.10}$$

The elastic modulus for the contact of a ball with inner raceway is

$$K_i = 2.15 \times 10^5 \sum \rho^{-\frac{1}{2}} (\delta_i^*)^{-3/2} \tag{3.11}$$

The elastic modulus for the contact of a ball with outer raceway is

$$K_o = 2.15 \times 10^5 \sum \rho^{-\frac{1}{2}} (\delta_o^{\cdot})^{-3/2} \tag{3.12}$$

The effective elastic modulus for the bearing system is given as

$$K = \left[\frac{1}{(1/k_i)^{1/n} + (1/k_o)^{1/n}} \right]^n \tag{3.13}$$

According to the equation (8), the total non-linear contact forces of the bearing in x and y directions is given by

$$f_x = k_b \sum_{j=1}^{N_b} \gamma_j \delta_j^n \cos \phi_j \tag{3.14}$$

$$f_y = k_b \sum_{j=1}^{N_b} \gamma_j \delta_j^n \sin \phi_j \tag{3.15}$$

where γ_j is switch function. The deformation of the ball takes place only when the ball is located in the load zone, and thereby non-linear contact force is produced. Switch function γ_j is given by

$$\gamma_j = \begin{cases} 1, & \delta_j > 0 \\ 0, & \delta_j \leq 0 \end{cases} \tag{3.16}$$

3.2.3 Fault Modelling of Rolling Element Bearing

When a defective (spalled) component, either a rolling element, an outer raceway or an inner raceway, interacts with its corresponding mating components, changes in contact stresses occurs. These change results into vibration, due to the deformation of rolling element. The deformation of the j^{th} rolling element over the site of the local fault is given by

$$\delta_j = (x_i - x_o) cos\phi_j + (y_i - y_o) sin\phi_j - C - \beta_j C_d \tag{3.17}$$

Now, to obtain the non-linear contact forces, equation (3.17) and (3.4) are substituted in equations (3.14) and (3.15). Then, solution of non-linear contact force is substituted into

dynamic equation of motion of bearing model. The solution of the non-linear coupled differential equation will give the vibration response of rolling element bearing with defect.

3.2.4 Modelling of outer race/ Inner race localized fault.

The major aspect of modelling the localized faults of rolling element bearing in this study is to test and verify the fault severity mathematically and experimentally for both the raceways. Unlike some of the previous models [4-10], which only obtained the vibration response for diagnosis of defect in a bearing for a single dimension of defect, this model obtains the vibration response of rolling element bearing with defect for three different dimensions of faults for both the raceway. The main purpose of obtaining the vibration spectra for three different dimensions of faults upon the raceway, is to understand and realized the change in vibration level of the bearing structure due to the severity of the fault.

The local fault on the surface of inner and outer races, is defined by the depth C_d over an angular distance of $(\Delta\phi_d)$ and it is modelled using the fault switch function β_j , so as to simulate the contact loss at a defined angular position (ϕ_d). The switch function β_j is defined as

$$\beta_j = \begin{cases} 1, & \phi_d < \phi_j < \phi_d + \Delta\phi_d \\ 0, & otherwise \end{cases}$$

The defect depth C_d plays an important role for assessment of fault severity. Three different values of C_d is used during simulation for both inner race and outer race, in order to evaluate the fault severity. Figure 3.2 shows the fault geometry of outer race defect.

The defect on outer race normally occurs in load zone and the outer race spall is fixed between the location ϕ_d & $\phi_d + \Delta\phi_d$.

The inner race spall rotates at the same speed of the rotor, since the rotor shaft is fixed to the inner race, i.e $\phi_d = \omega_s t + \phi_{d0}$, where ϕ_{d0} is the initial starting location of the spall.

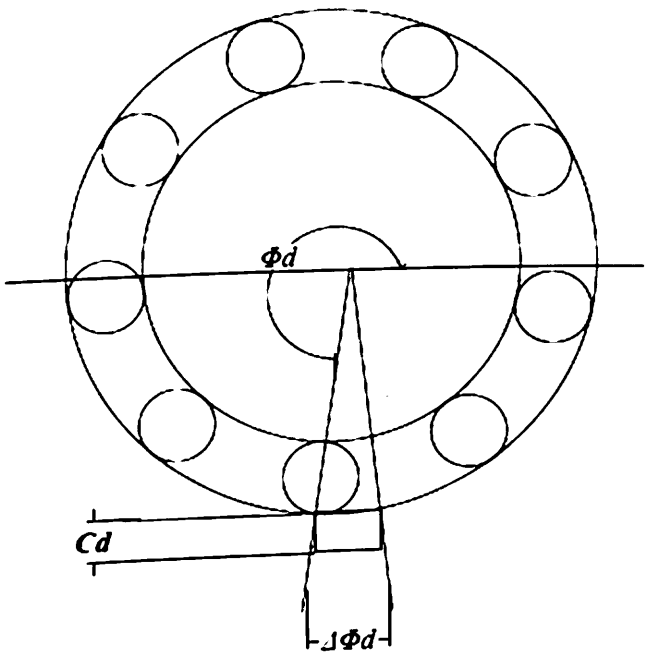

Figure 3.2 Outer race defect geometry

3.2.5 Modelling of ball fault.

A spall is considered on one of the rolling elements (rolling element K), which rotates at the speed as that of rolling element. The rotational frequency of the rolling element is termed as ball spin frequency i.e ω_{spin}, which is defined as

$$\omega_{spin} = \frac{\omega_s}{2}\frac{D_p}{D_b}\left(1 - \left(\frac{D_b}{D_p}cos\alpha\right)^2\right) \tag{3.18}$$

The position of the spall (ϕ_s) is defined as

$$\phi_s = \omega_{spin}t + \phi_{d0} \tag{3.19}$$

where, ϕ_{d0} is the initial position of the spall.

The position of spall is dependent upon the speed of the rolling element; thus, it is a function of shaft speed. Thereby, rolling element faults share similar characteristics with faults on inner race and different from the faults on the outer race due to its fixed location.

Contact loss between the rolling element and raceway is detected only for the faulty rolling element K and this happens twice for each complete rotation of the rolling element i.e first when it is in touch with inner race and second, when it is touch with outer race.
Due to the difference in curvature between the two races, the switch values and periods of switching on ($\Delta\phi_d$) will not be same for both races. The inner race will make deep and long contact compared to that of outer race. Instead of defining two different spall geometries, the fault switch function β_j is defined in such a way to show the variation as sensed by two races. β_j is given by

$$\beta_j = \begin{cases} 0 & if\ 0 < \phi_s < \Delta\phi_{d0} \quad j \neq k \\ 1 & if\ pi < \phi_s < (pi + \Delta\phi_{di})\ j = k \\ \frac{C_{dr}+C_{di}}{C_{dr}-C_{di}} & otherwise \\ 0 & \end{cases} \tag{3.20}$$

The derivation of the switch values is described in Figure3. It is divided into two cases. First case describes about the contact between the spalled rolling element and inner race. For this case, the total loss of contact occurs as a result of creating a slot of width 2x, which is the summation of two values. The maximum depth the inner race will reach the slot region is as described in equation (3.21). This equation represents the movement of the inner race from its original contact position- moving downward.

The second is the maximum contact loss in the rolling element contact as a result of the spall given in equation (3.22) (C_{dr} represents slot created upon the rolling element- moving upwards).

Now, second case describes the contact of rolling element with outer race. In this case, the net change in the contact (C_d) is the difference between the rolling element movement (C_{dr}) and outer race movement (C_{d0}) as shown in equations (3.22) & (3.24).

The reason for this movement is that outer race moves downwards and so does the ball, which comprises the meaning that the net change in the contact between the original and the new contact position can be obtained by subtracting two changes.

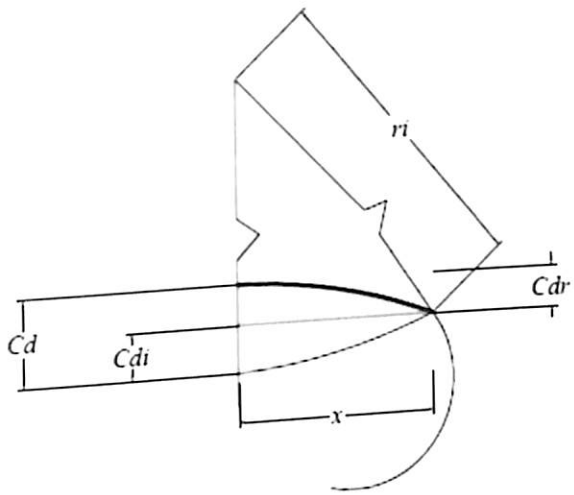

Figure 3.3 Ball spall depth as sensed by inner race

$r_i = \frac{D_P - D_b}{2}$ (Inner race radius)

$x = \Delta\phi_d \frac{D_b}{4}$ (Half the spall width)

$C_{di} = ri - \sqrt{ri^2 - x^2}$ (Maximum depth the inner race will reach) (3.21)

$$C_{dr} = \frac{Db}{2} - \sqrt{\left(\frac{Db}{2}\right) - x^2} \quad (3.22)$$

(Maximum contact loss in the rolling element contact as a result of spall)

Similarly, $ro = \frac{Dp+Db}{2}$ (outer race radius) (3.23)

$Cdo = ro - \sqrt{ro^2 - x^2}$ (3.24)

(Maximum depth the outer race will reach)

Angular widths of the fault also depend upon the races (inner and outer) contacting the spalled roller and are given as

$\Delta\phi do(rad) = \frac{2x}{ro}$ (3.25)

(Angular width of the fault sensed by outer race)

$\Delta\phi di(rad) = \frac{2x}{ri}$ (Angular width of the fault sensed by inner race). (3.26)

3.3. Rotor-bearing experimental setup.

The experimentation is performed upon the bearing to test its fault severity by using the dedicated experimental setup. The schematic of setup is as shown in Figure 3.4 and picture representation of setup is shown in Figure 3.5. The setup consists of synchronous 3-phase servo AC motor. Experimentations are carried upon both defective and healthy bearing. The bearing of given specifications as shown in Table3.1 is used for experimental analysis. The defects of three different sizes as mentioned in Table3.2 are introduced upon the surface of outer race and inner race using electric discharge machining (EDM) technique. While, a single point notch is created as a defect upon one of the balls of bearing by using same EDM method. The photographs of sample defects upon the inner race, outer race and ball are shown in Figure 3.6.

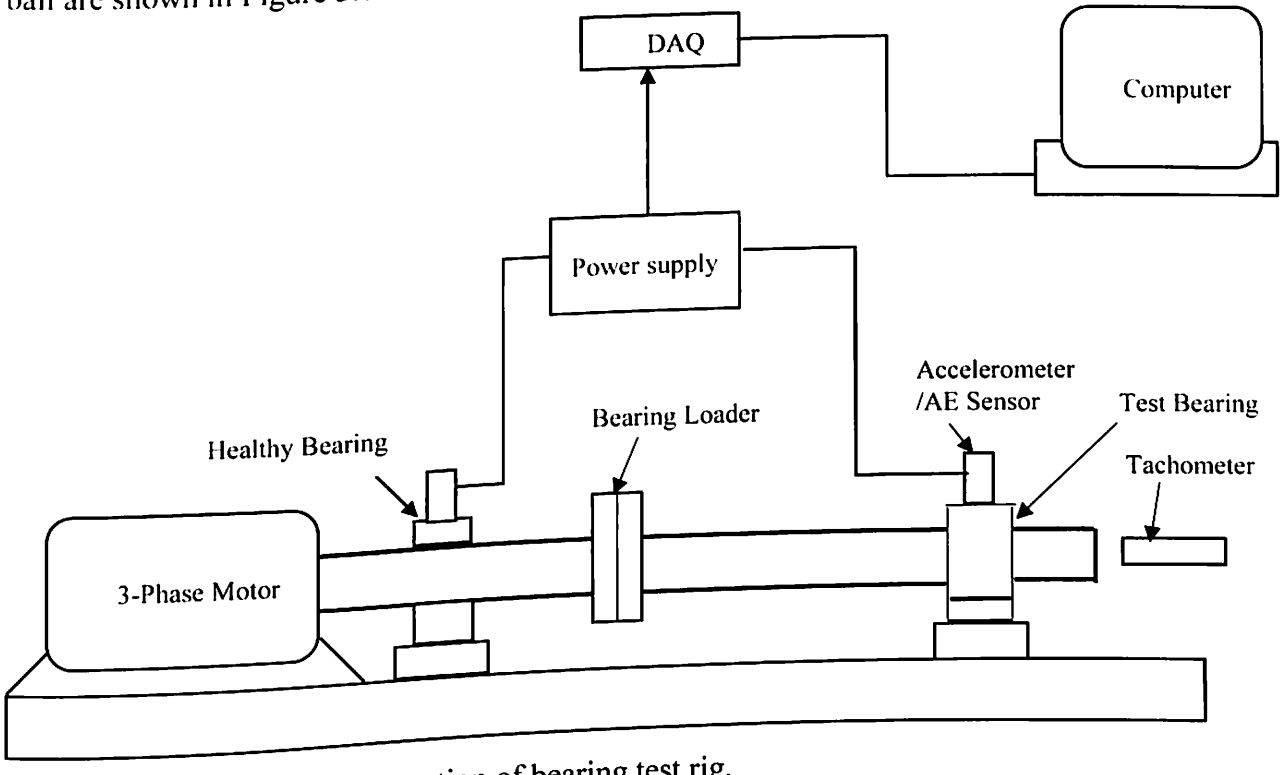

Figure 3.4 Schematic representation of bearing test rig.

To obtain the vibration response generated by the defective bearing, tri-axial accelerometer (model: industrial ICP accelerometer 8076K) with sensitivity of 102.0 mv/g is placed vertically upon the housing of defective bearing. The vibration data is recorded using 8 channel OROS multi-analyzer. The target of the experimental analysis is to obtain the fault characteristic frequency by processing the vibration signal. Table 3.3 shows the calculated

fundamental defect frequencies of components of bearing used in experiment. The radial load of 50N is applied in vertical direction. Here the constant rotational frequency of 25 Hz is used for performing experimental analysis.

Figure 3.5 Bearing Test Rig 1. Defective Bearing 2. Accelerometer 3. Loader 4. Healthy Bearing.

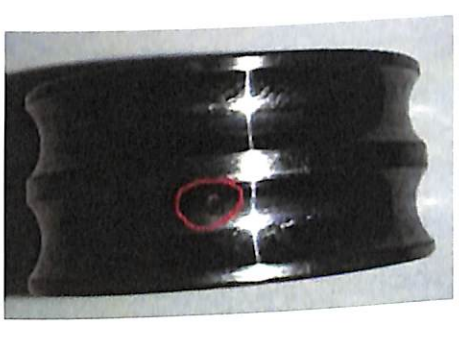

(a)

(b)

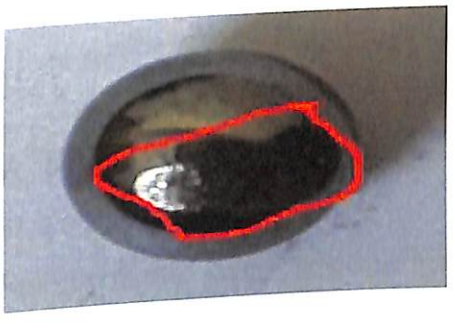

(c)

Figure 3.6 Photographs of defects (a) Inner race (b) Outer race (c) Ball

Table 3.1 Rolling Element Bearing Specification.

Bearing No	ETN 9 1204
Number of balls N	12
Pitch Diameter (PD)	34.44 mm
Ball Diameter (BD)	7.12 mm
Contact angle (α)	0^0
Mass of inner race and shaft(m_i)	1.507 Kg
Mass of outer race and housing(m_o)	1.043 Kg
Mass of unit resonator(m_r)	1 Kg
Stiffness of outer race (K_o)	3.13×10^5 N/m
Stiffness of inner race (K_i)	1.47×10^5 N/m
Stiffness of unit resonator (K_r)	8.88×10^9 N/m
Contact stiffness (K_h)	7.06×10^4 N/m
Damping of Outer race (C_o)	2210.7 Ns/m
Damping of inner race (C_i)	1376.8 Ns/m
Damping of unit resonator (C_r)	9424.8 Ns/m

3.4. Numerical simulation and Experimentation results.

The developed model is used to simulate the vibration response of the rolling element bearing for the localized outer race, inner race and rolling element fault, to test and verify the fault severity. The rotational frequency of the shaft is set to $\omega_s = 25$ rad/s^2. The vibration signals are processed for frequency and time-frequency domain. Here, the study is divided into different cases for accessing the fault severity, which is as follows

Case1) Outer race and inner race with three different fault sizes.

Case2) Rolling Element with single point defect.

It is important to consider these two cases since the occurrence of faults are inevitable at this component of rolling element bearing. These faults are related to operational wear of rolling element bearing and becomes severe with due course of time. Therefore, to study the effect of fault severity upon the vibration response of rotor-bearing system, it is divided

into two cases. The three dimensions of fault as mentioned are used for understanding the vibration response of the bearing structure due to the change in fault sizes upon the surface of outer race and inner race, to determine and understand the concept of severity of the fault in rotor dynamic system. The vibration response due to the different fault sizes is evaluated for both simulation and experimentation for different cases.

The key indicator of the presence of the fault in the frequency domain is the characteristic defect frequencies. The characteristic defect frequencies depend upon the rotational frequency of the shaft and the location of the defect in the bearing [5]. The expressions for the characteristics defect frequencies for various defects of the bearing is given in equation (3.27), where D_b is the ball diameter, D_p is the pitch diameter, f_s is the shaft's rotational frequency. Table 4 shows the good co-relation between the calculated and identified fault frequencies along with amplitude for the analyzed bearing at constant rotational speed which was observed experimentally.

Ball Pass Frequency Outer Raceway

$$f_{bpfo} = \frac{f_s \times N_b}{2}\left(1 - \frac{D_b}{D_p}cos\alpha\right) \qquad 3.27(a)$$

Ball Pass Frequency Inner Raceway

$$f_{bpfi} = \frac{f_s \times N_b}{2}\left(1 + \frac{D_b}{D_p}cos\alpha\right) \qquad 3.27(b)$$

Ball Spin Frequency

$$f_{bsf} = \frac{f_s}{2} \times \frac{D_p}{D_b}\left[1 - \left(\frac{D_b}{D_p}cos\alpha\right)^2\right] \qquad 3.27(c)$$

To detect the faults in a bearing, conventionally, frequency-based techniques are used to diagnose the bearing faults. However, frequency-based techniques are not suitable for the analysis of non-stationary signals that are related to the bearing fault. Non-stationary signals can be analyzed by using time-frequency domain techniques such as short-time fourier transform, the wavelet transform (WT) and the Hilbert-haung transform. Among different time-frequency techniques, WT is the popular time-frequency techniques due to the flexible and multi-resolution solution than the short time fourier transform. WT is

classified as the continuous WT(CWT), the discrete WT(DWT) and wavelet packet analysis.

In this study of bearing fault diagnostic, CWT transform is used. CWT based classification of the fault is best suited for noisy data occurring from the defective bearing. The small amplitudes of vibration response produced by the defective bearing in a high-frequency band is to be known prior to the wavelet analysis. Sym 12 wavelet is chosen to be the best mother wavelet to perform the CWT analysis.

Table 3.2 Bearing Fault Sizes.

Fault size(mm) ($L_{defect} \times W_{defect} \times D_{defect}$)	Location	Name of fault
1.0×0.5×0.3	Outer race	OR1
1.0×0.5×0.3	Inner race	IR1
1.0×0.75×0.5	Outer race	OR2
1.0×0.75×0.5	Inner race	IR2
1.0×1.0×0.75	Outer race	OR3
1.0×1.0×0.75	Inner race	IR3
0.5×0.5×0.5	Ball	Ball fault

Table 3.3 Calculated defect frequencies of bearing components at 1500 RPM

Rotational Frequency(f_s)	25 Hz
Outer race defect frequency (f_{bpfo})	118.9 Hz
Inner race defect frequency (f_{bpfi})	181 Hz
Ball spin frequency (f_{bsf})	57.438 Hz

3.4.1 Healthy bearing analysis

Rolling element bearing components generates vibration response signal due to the change in speed of the shaft rotation. A healthy bearing with well lubrication and properly installed

also generates vibrations due to the time-varying distribution of balls relative to the inner and outer races. Figure 3.7 shows the time domain signal for both simulated and experimental vibration response. Figure 3.8 shows the FFT spectrum for both simulated and experimental vibration response. From Figure 3.8, it clearly reflects that there is a dominant peak at shaft frequency 25 Hz.

The CWT plot for both simulated and experimental response of healthy bearing is shown in Figure 3.9. The time interval T=0.038300 sec at simulated CWT and T= 0.041600 sec at experimental CWT, between two consecutive amplitudes indicates the high frequency excitation.

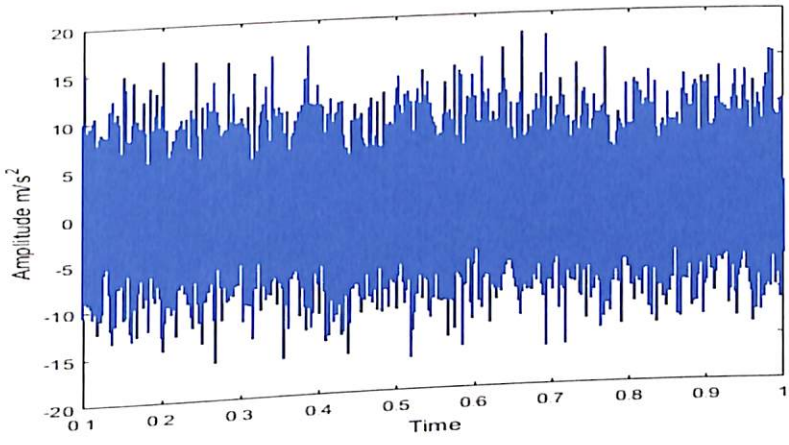

(a)

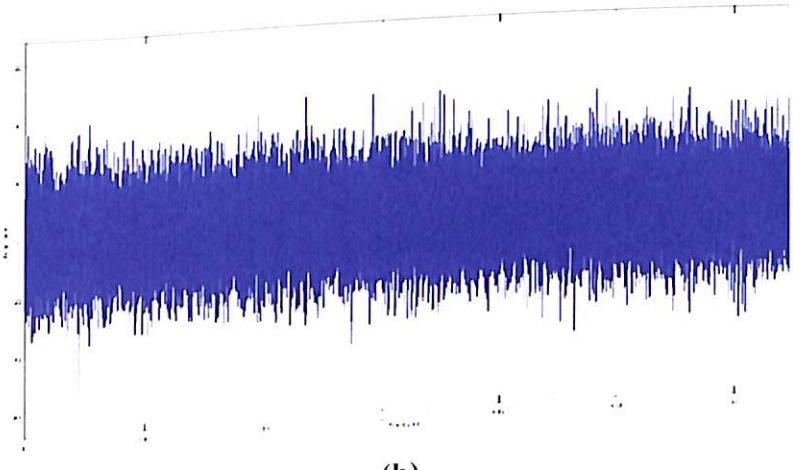

(b)

Figure 3.7 (a) Simulated time domain plot of healthy bearing
(b) Experimental time domain plot of healthy bearing.

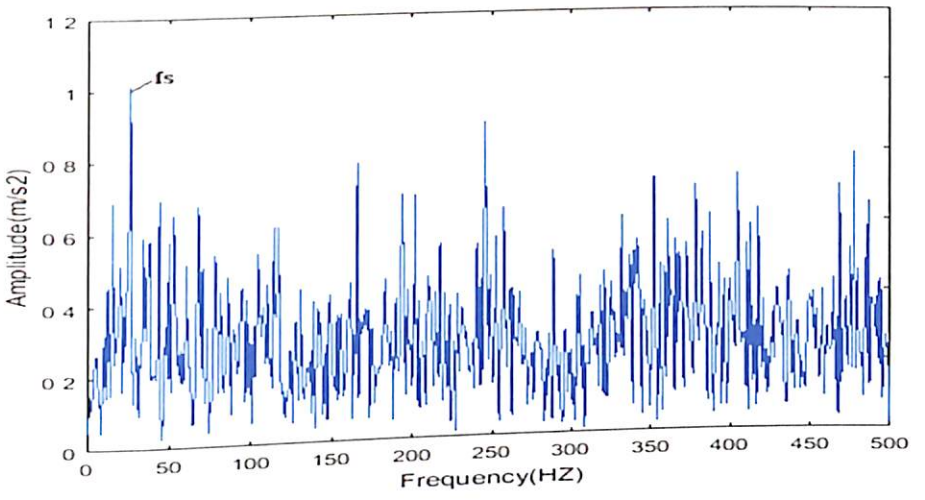

(a)

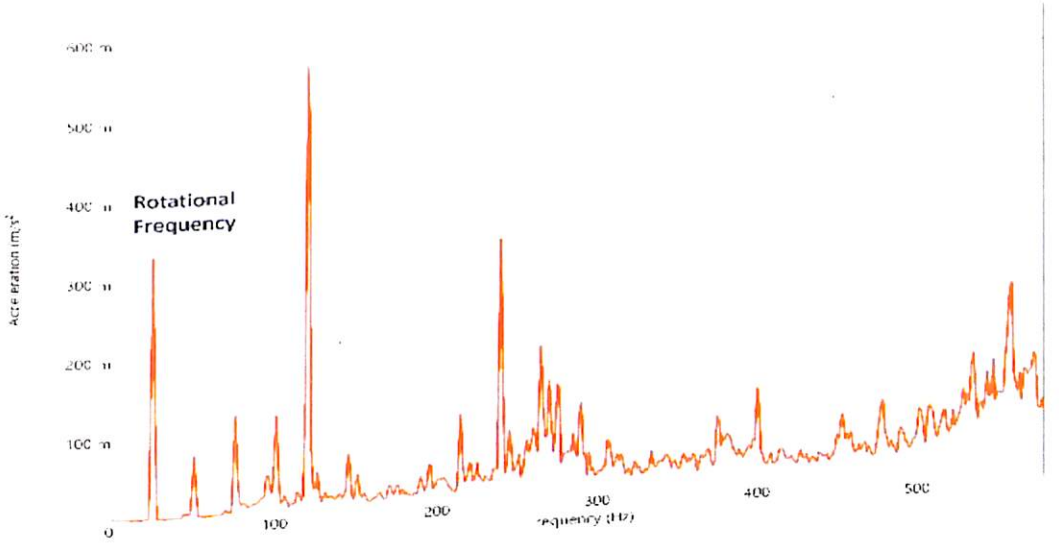

(b)

Figure 3.8 (a) Simulated FFT of Healthy Bearing.

(b) Experimental FFT of Healthy Bearing.

The time interval 'T' corresponds to shaft's rotational frequency of 25 Hz. The CWT plot clearly shows the small amplitudes of vibration, which is due to the varying position of ball and application of the radial load. This small amplitude of vibration indicates that there is no presence of fault in bearing.

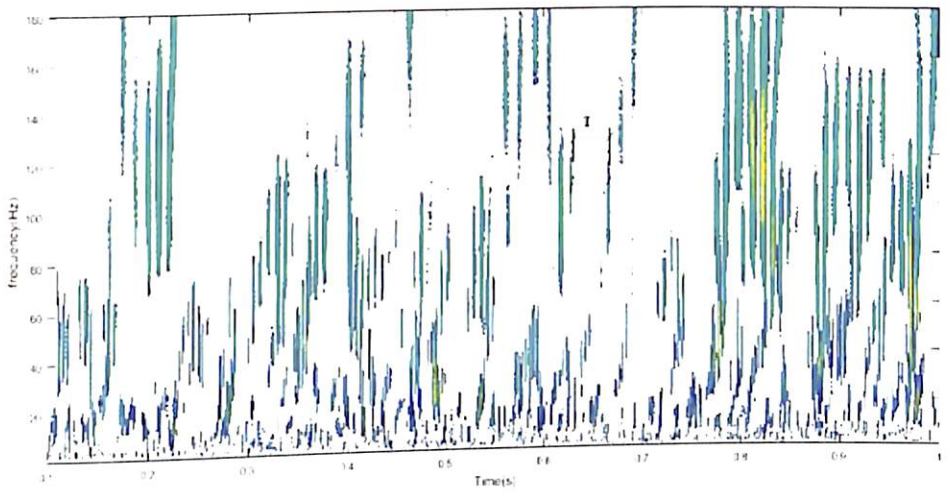

(a)

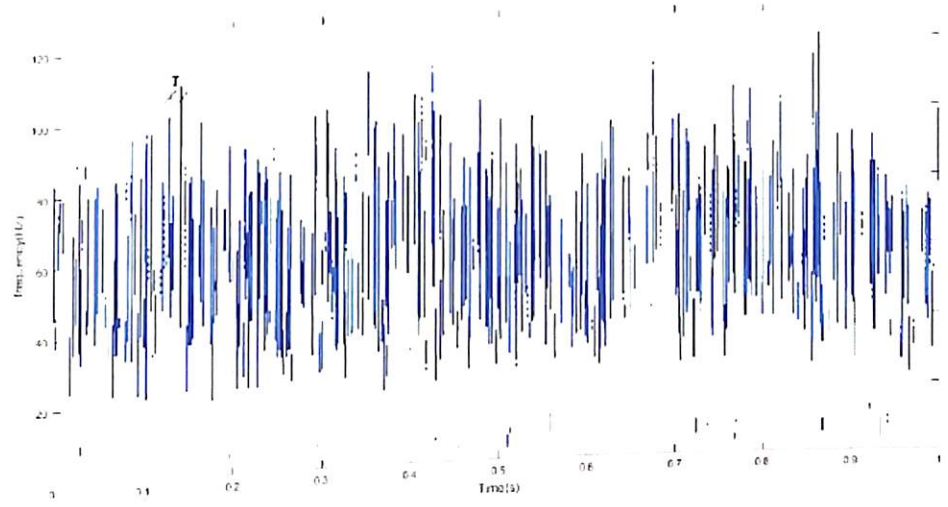

(b)

Figure 3.9 (a) Simulated Time-Frequency Plot (CWT) of Healthy Bearing.

(b) Experimental Time-Frequency Plot (CWT) of Healthy Bearing.

3.4.2 Outer race fault analysis

Figure 3.10 shows the time domain signals for both simulated and experimental response of outer race defect. The time domain signals are highly impulsive in nature due to the interaction of each roller with the fault on the surface of outer race, while passing through the loading zone. This results into dominant characteristic outer race defect frequency. The high frequency components are observed in time domain signal due to the presence of

defect. There is a good agreement between the simulated and experimental time domain signal in terms of pattern and scales. Here time domain signal for OR3 is presented. Time domain signal does not provide the information about the defect frequency, since it is completely masked by noise. FFT and time -frequency technique CWT is performed upon both the simulated and experimental vibration response, for potential diagnosis of outer race fault and its severity.

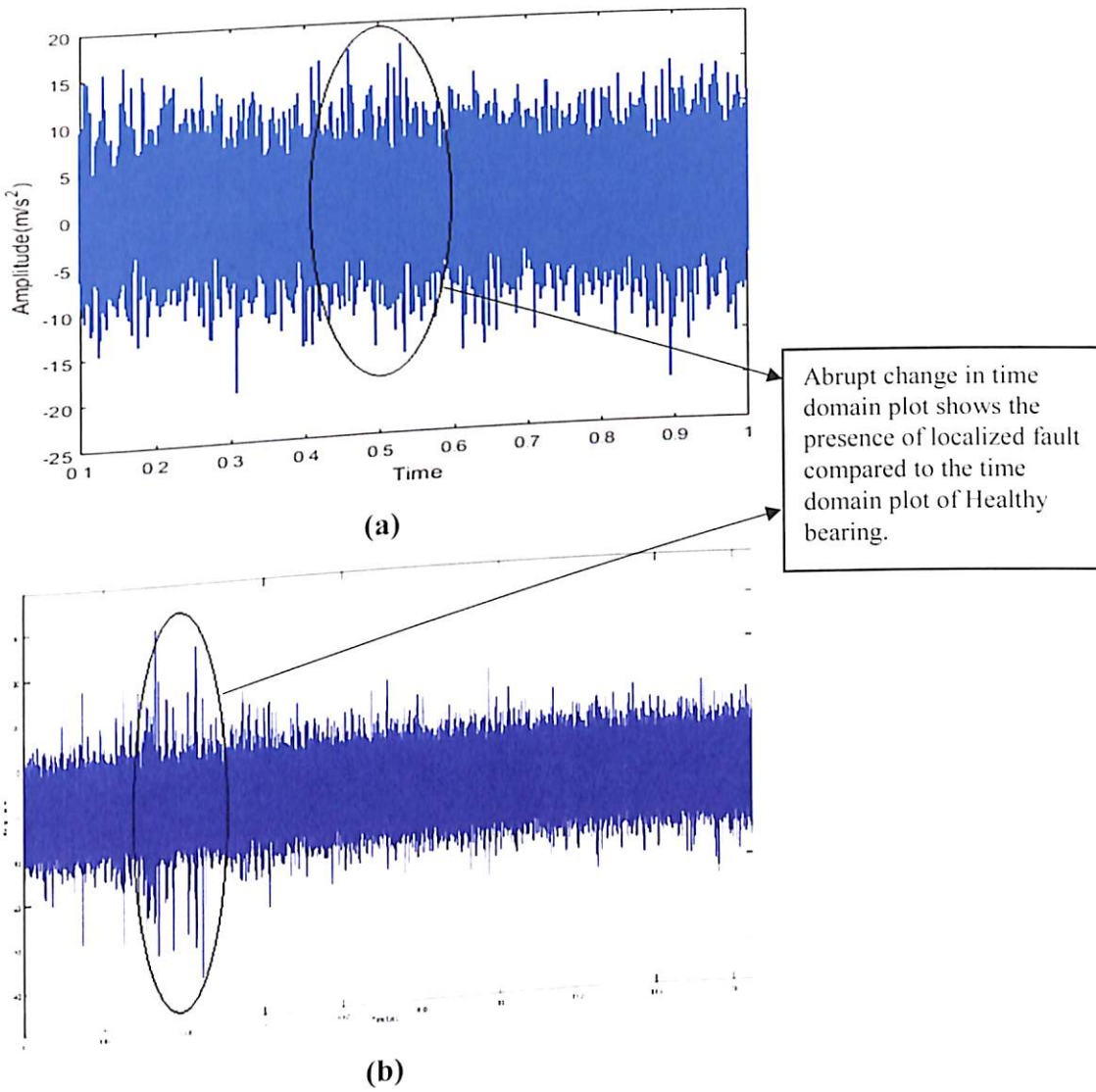

Figure 3.10 (a) Simulated time domain plot for outer race defect- OR3.

(b) Experimental time domain plot for outer race defect -OR3.

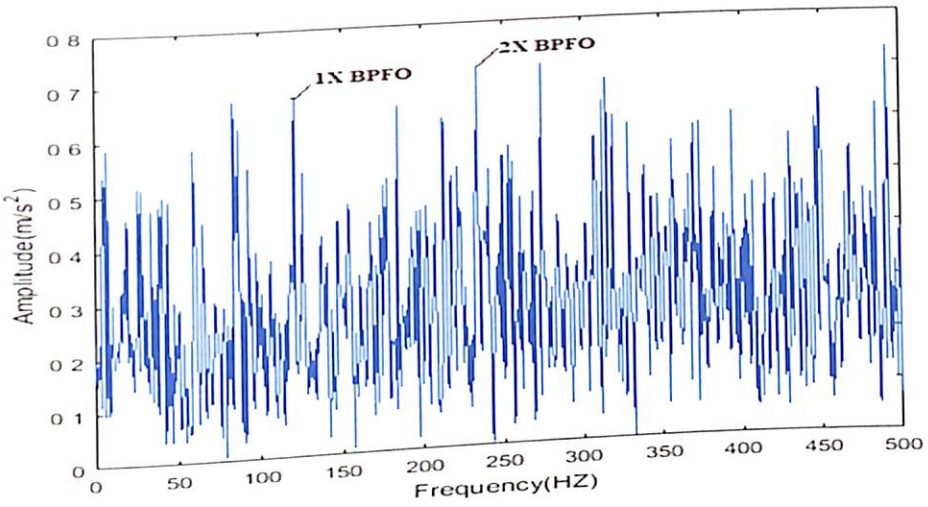
1X BPFO
2X BPFO
Amplitude(m/s²)
Frequency(HZ)
0 8
0 7
0 6
0 5
0 4
0 3
0 2
0 1
0
0 50 100 150 200 250 300 350 400 450 500

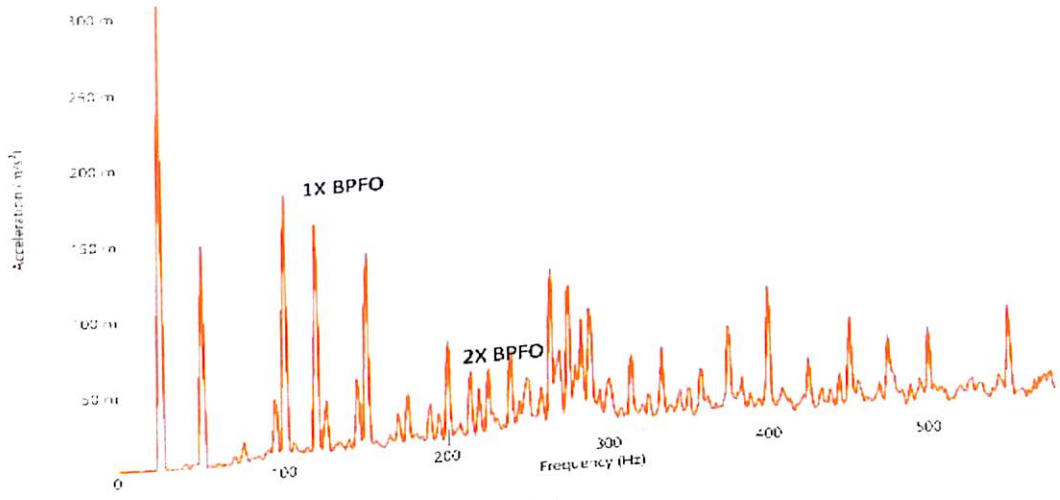
1X BPFO
2X BPFO
Frequency (Hz)

(a)

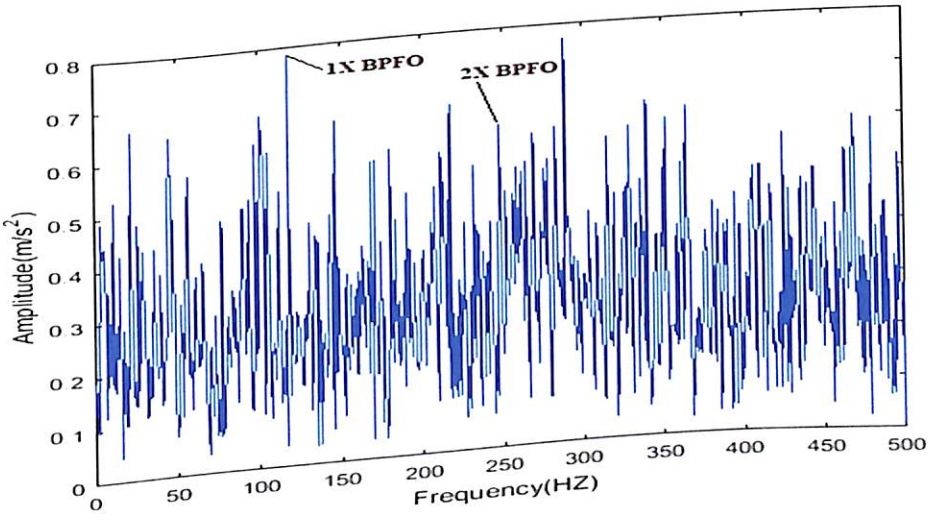
1X BPFO
2X BPFO
Amplitude(m/s²)
Frequency(HZ)
0 8
0 7
0 6
0 5
0 4
0 3
0 2
0 1
0
0 50 100 150 200 250 300 350 400 450 500

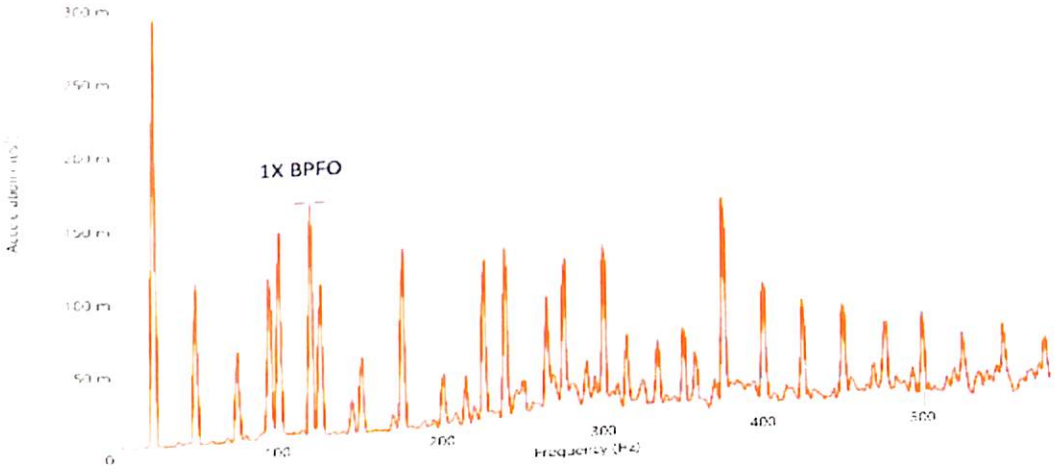

(b)

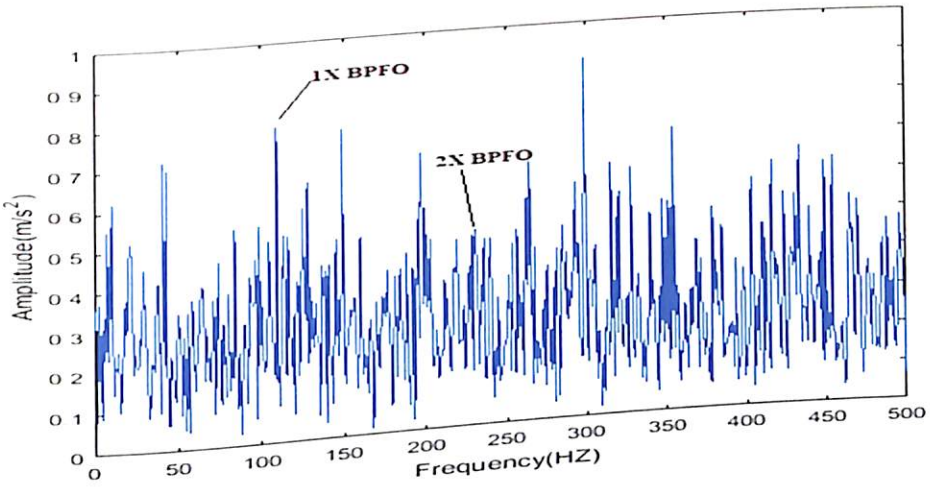

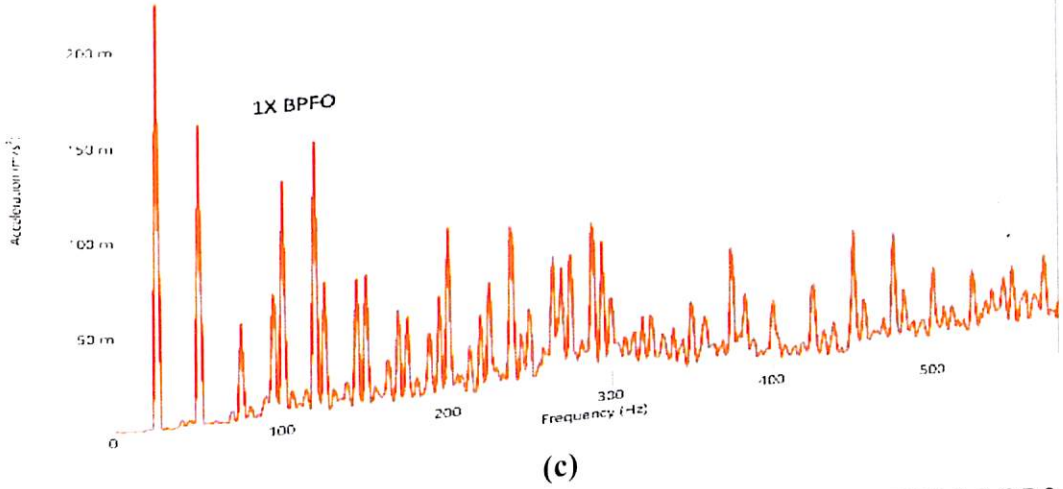

(c)

Figure 3.11 Simulated and Experimental FFT of outer race defect (a) OR1 (b) OR2 (c) OR3.

Figure 3.11 shows the FFT for simulated and experimental vibration response, for different defect sizes, to understand impact of the fault severity upon the level of amplitude in the system. Figure 3.11 clearly shows the dominant peak of amplitude at outer race defect frequency f_{bpfo}= 118.9 Hz and its second harmonic $2f_{bpfo}$= 233.1 Hz. From Figure 3.11, as the size of the fault increases, the level of amplitude also increases corresponding to the outer race defect frequency. This indicates the presence of fault and provide the significant analysis of fault severity due to the change in amplitude level. CWT analysis of both simulated and experimental response is shown in Figure3.12. CWT clearly indicates the intensity and frequency of the defect. CWT combines the advantages of the time-scale and frequency domain features and provide more information upon the defect feature.

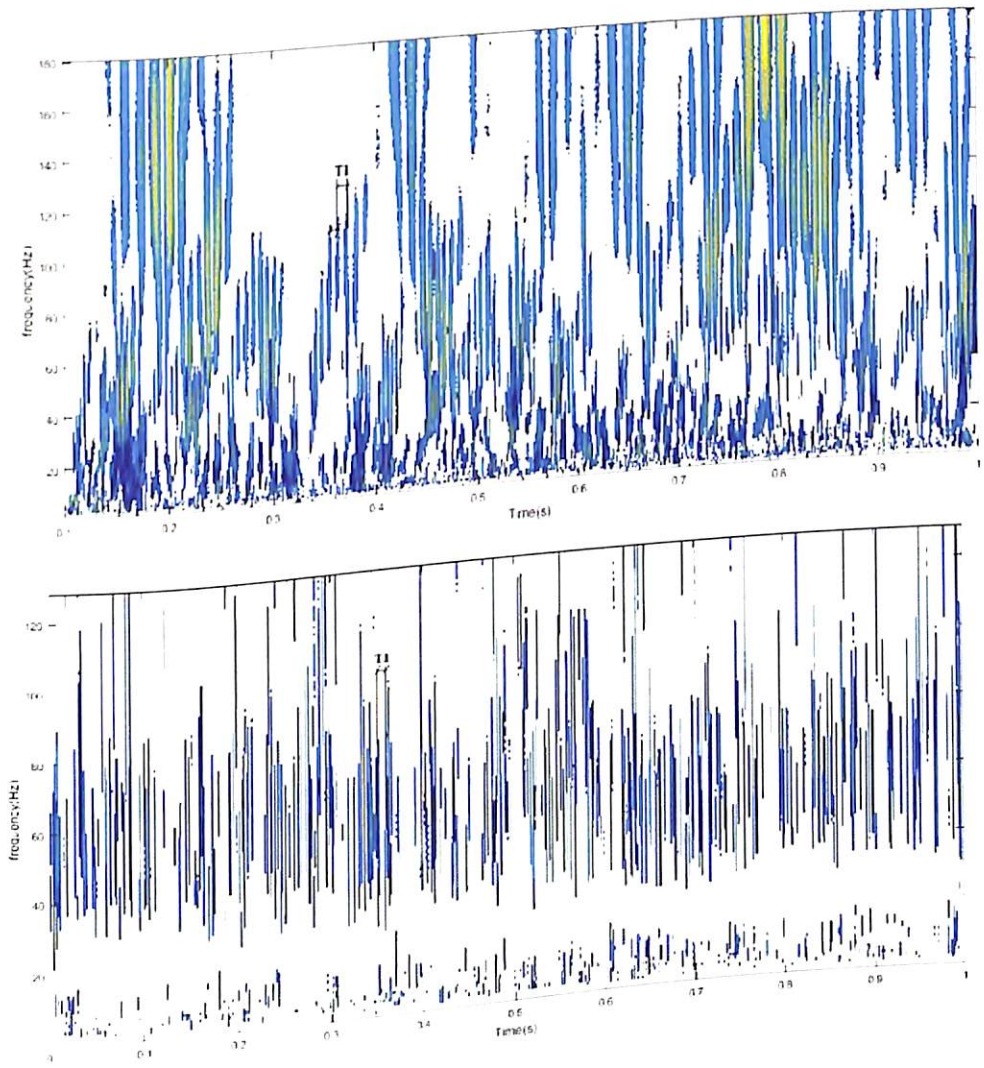

(a)

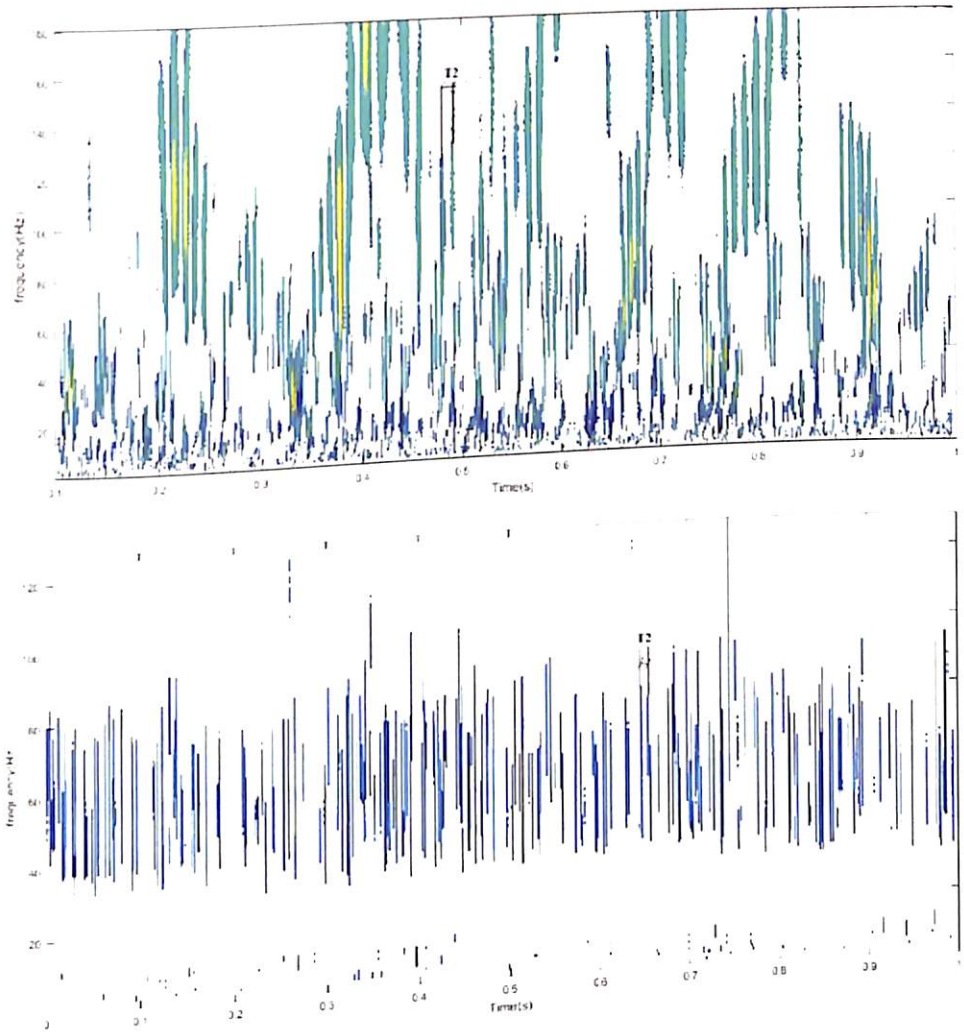

(b)

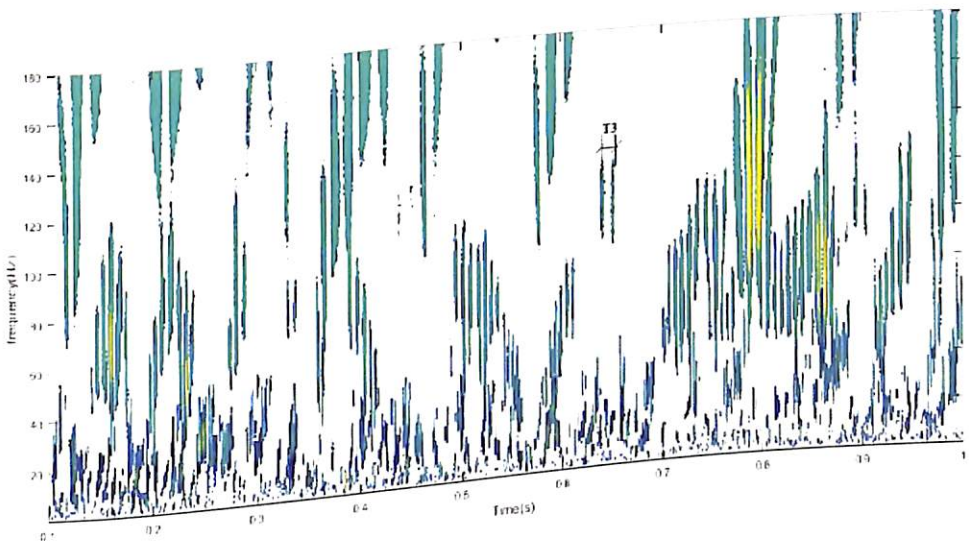

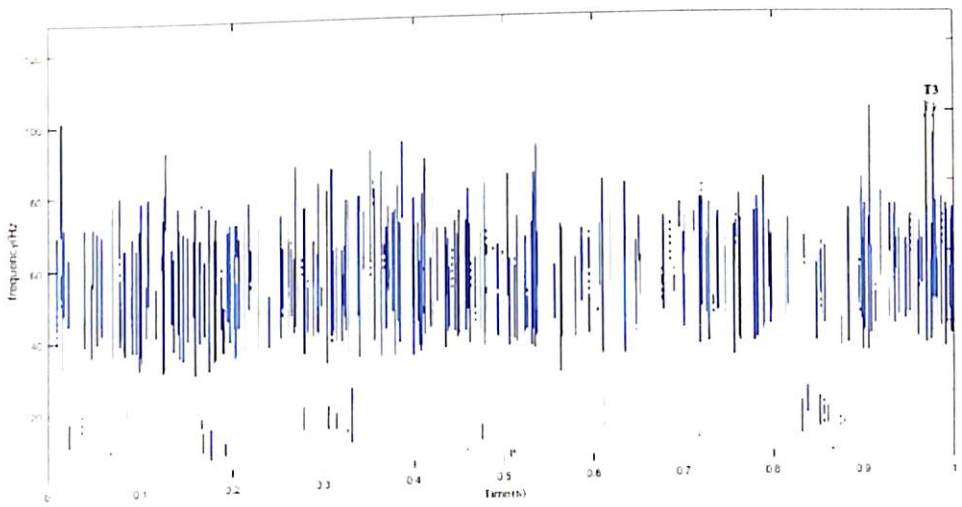

(c)

Figure 3.12 Simulated and Experimental CWT of outer race defect (a) OR1 (b) OR2 (c) OR3.

From the CWT plot, the existence of the high-frequency components is observed with repetitive occurrence. This clearly indicates the presence of the fault. The time interval T1=T2=T3=0.084sec of simulated CWT and T1=T2=T3=0.0085 sec of experimental CWT corresponds to the characteristic outer race defect frequency of 118.1 Hz. From the CWT analysis, it is observed, that the distance of time interval increases as the defect size increases. This clearly indicates the severity of fault of outer race.

3.4.3 Inner race fault analysis

Similar to the fault of outer race, an inner race fault was also introduced for three different defect sizes as that of outer race. The defect on the inner race will rotate along with the rotation of shaft's speed and will pass through the loading zone each cycle. Vibration response will be high when the defect present upon the surface of inner race interacts with its mating component in the loading zone. However, when defect will be on the top position of inner race, the rolling elements will miss the defect and this results into shifting of faulty frequency into lower bands. Thereby, detecting the fault in case of inner race is challenging task than a fixed race. Figure 3.13 shows the time domain vibration response for both simulated and experimental response. Here also, time domain signal for IR3 is presented.

It is quite obvious, that there is a similarity between simulated and experimental response in terms of impact pattern. Here large impacts are observed when inner race goes through the load zone. The FFT spectrum shown at Figure 3.14 indicates a shaft frequency peak at 25 Hz. The characteristic frequency of inner race defect(f_{bpfi}) is 181 Hz and its second harmonic ($2\,f_{bpfi}$) is 362 Hz, which is clearly observed in FFT spectrum. The CWT plots of inner race defect for all defect sizes are shown in Figure 3.15, reveals the existence of repetitive high-frequency components which indicates the presence of the fault on inner race. The spectrum of both simulated and experimental results of vibration response appears only when the inner race is in load zone. The patterns of frequency components in CWT plots varies for all defect sizes for both simulated and experimental results. The time intervals T1=T2=T3=0.0055sec of simulated cwt and T1=T2=T3=0.0056 sec of experimental cwt corresponds to the characteristic inner race defect frequency of 181.1 Hz. It is clear that cwt technique detects the presence of inner race fault and provides the strong approach of determining fault severity.

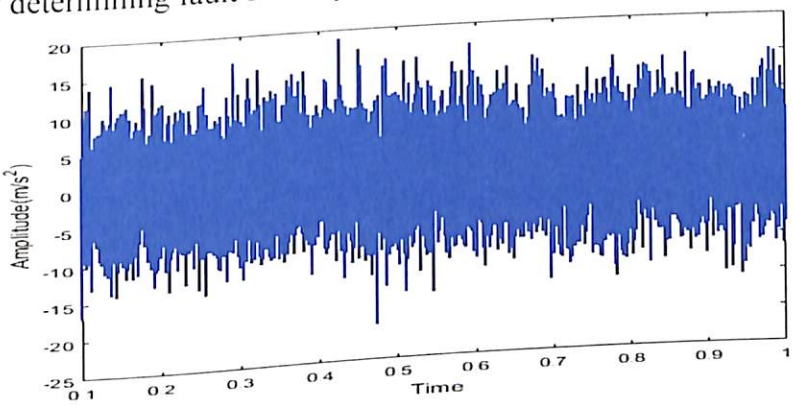

(a)

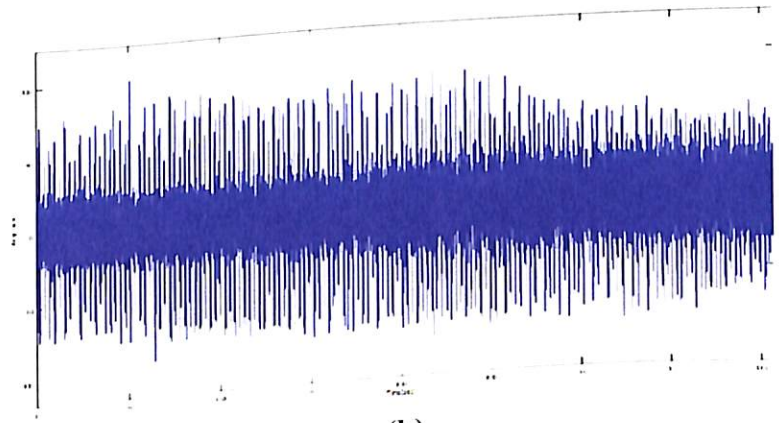

(b)

Figure 3.13 (a) Simulated and **(b)** Experimental time domain plot of inner race defect -IR3

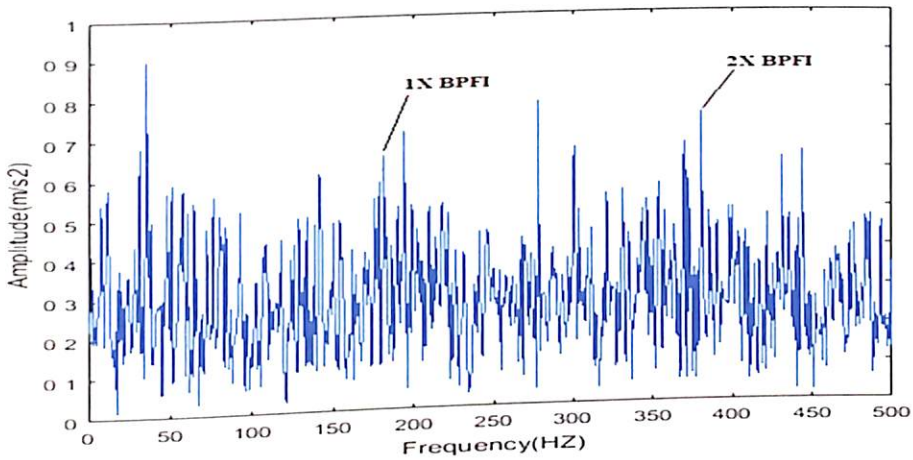
1X BPFI
2X BPFI
Amplitude(m/s2)
Frequency(HZ)

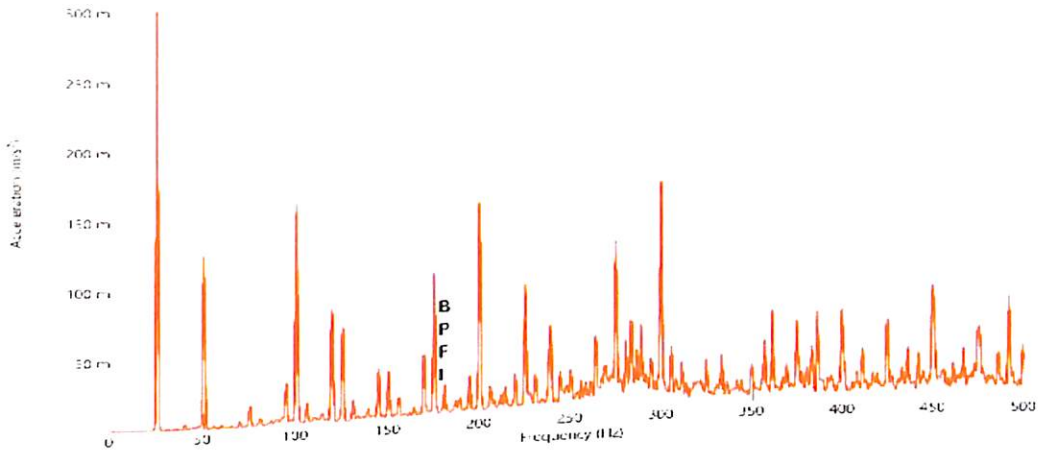
B
P
F
I

(a)

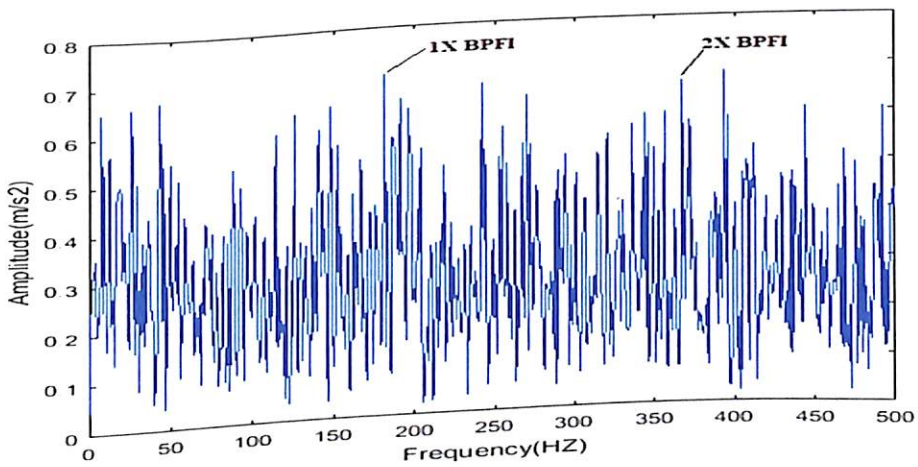
1X BPFI
2X BPFI
Amplitude(m/s2)
Frequency(HZ)

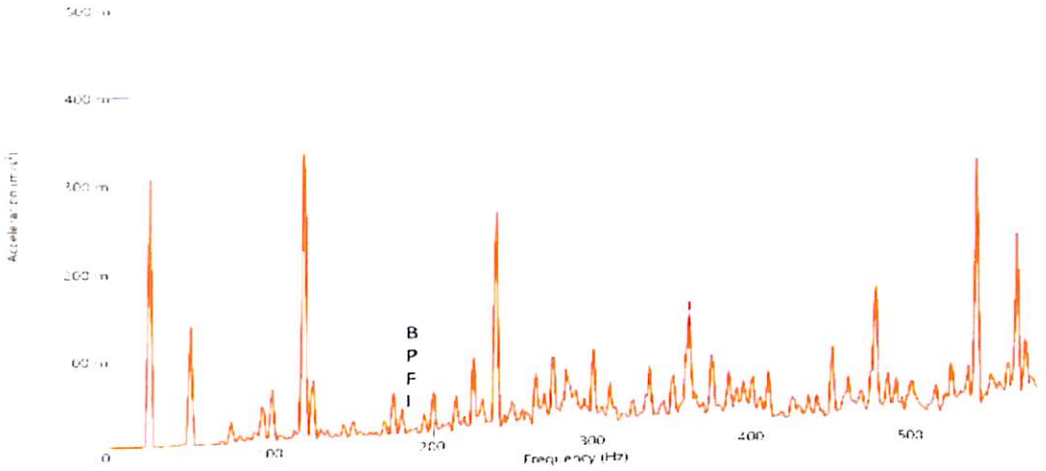

(b)

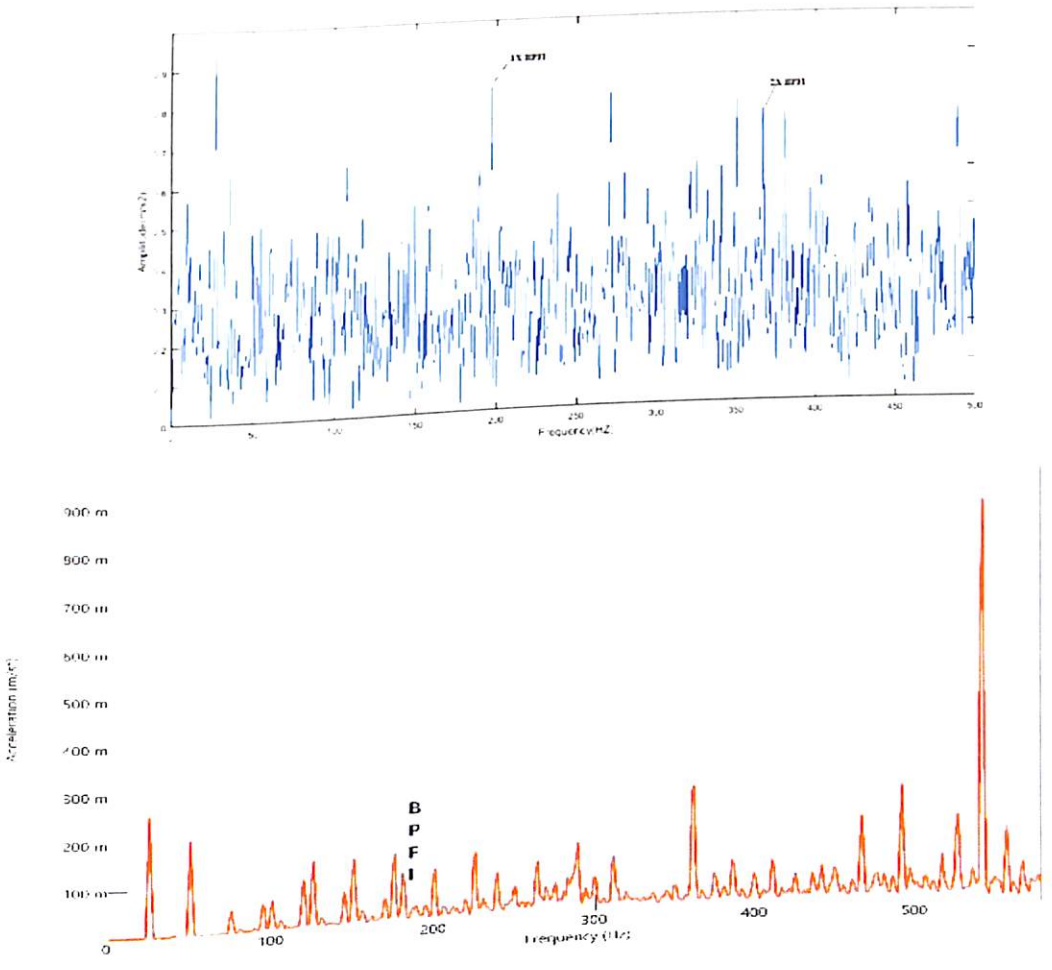

(c)

Figure 3.14 Simulated and Experimental FFT of inner race defect (a) IR1 (b) IR2 (c) IR3

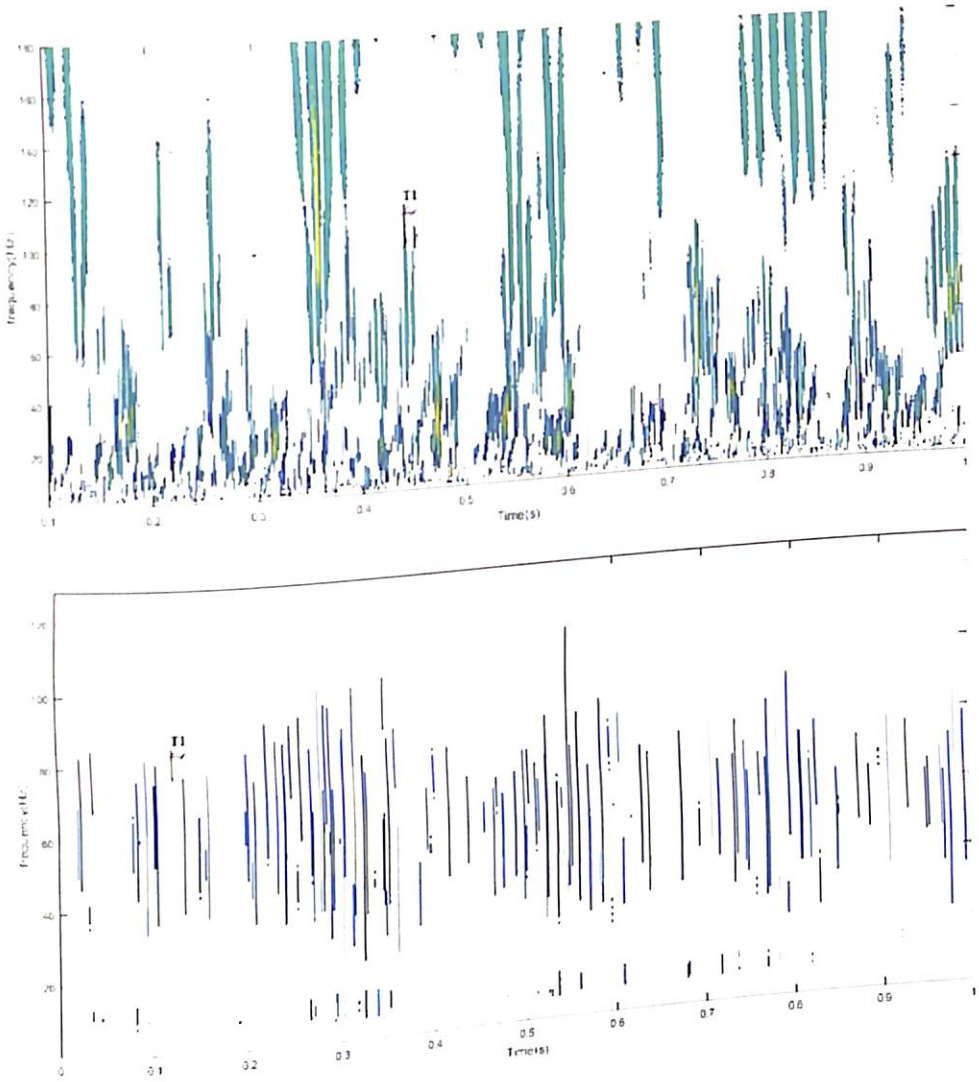

(a)

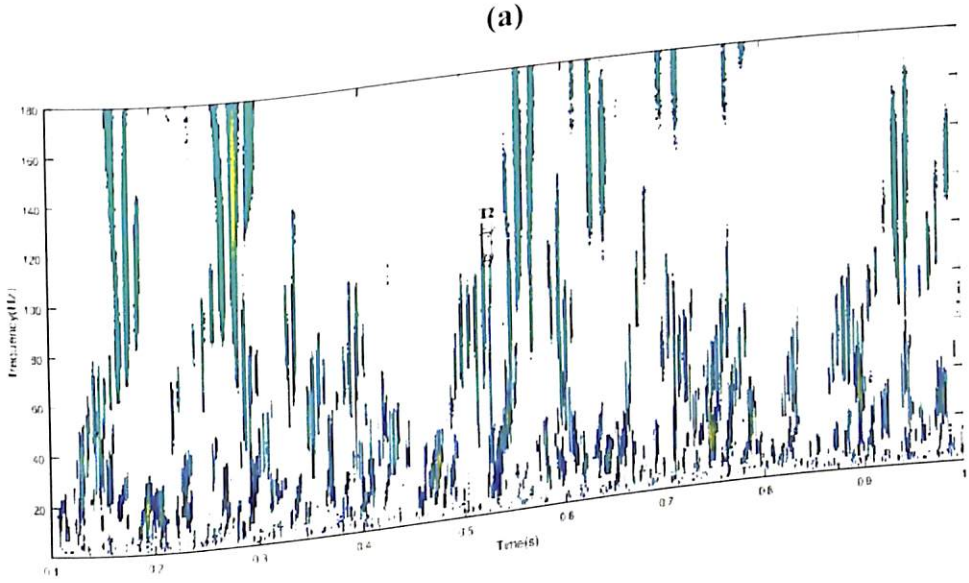

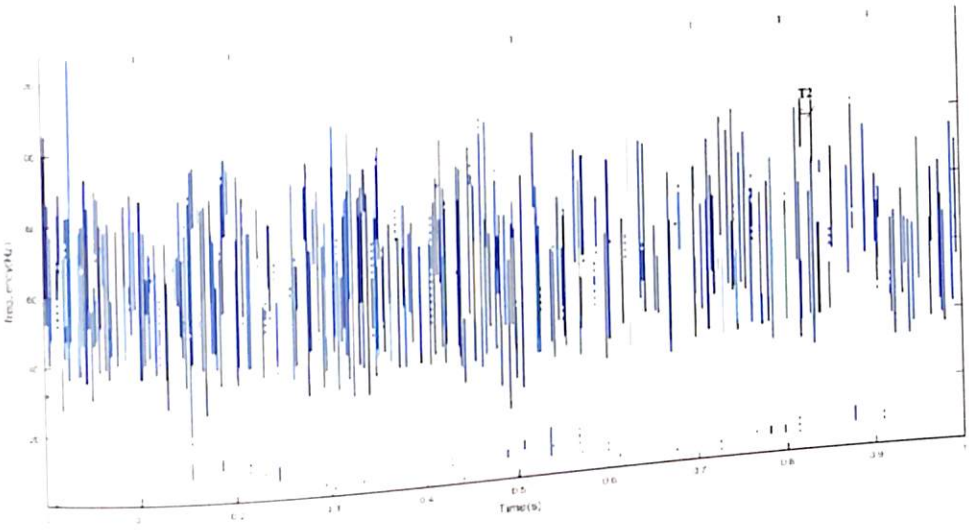

(b)

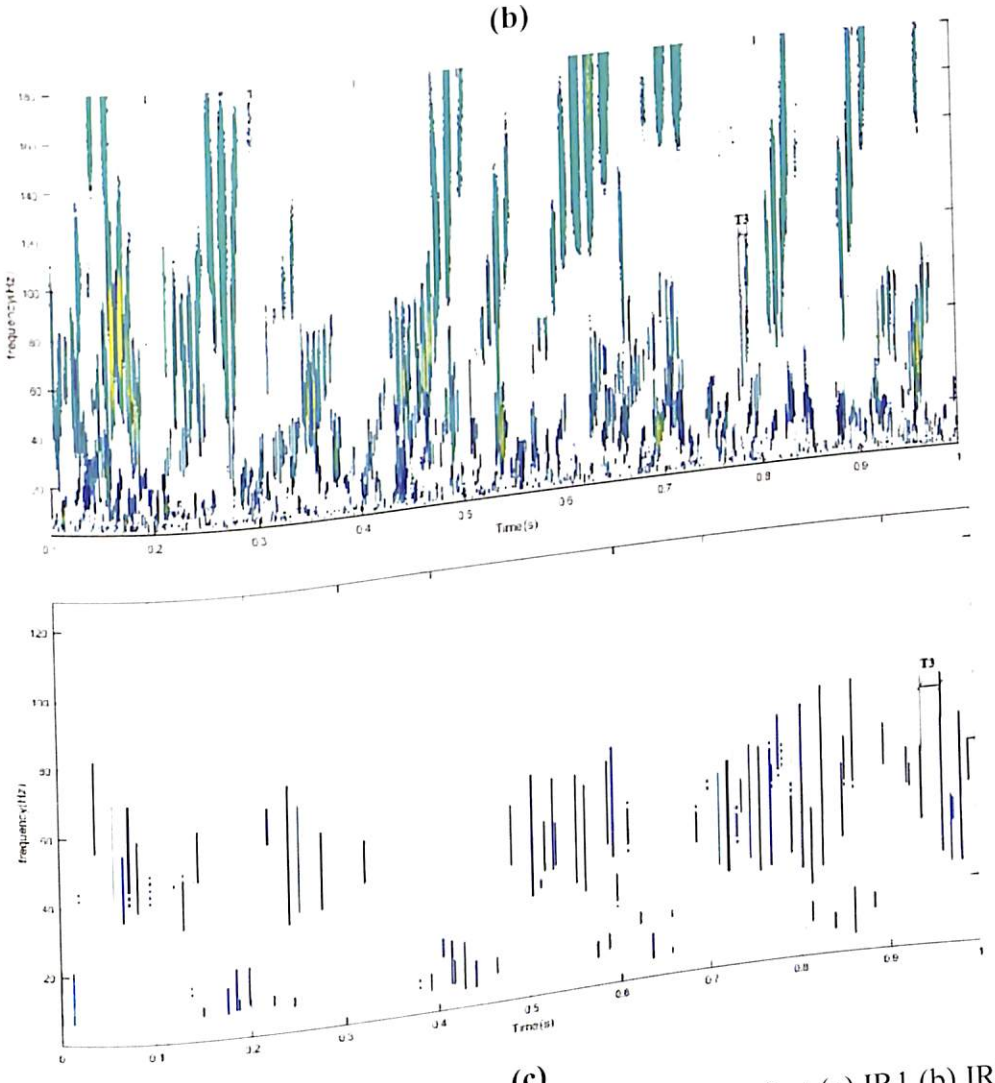

(c)

Figure 3.15 Simulated and experimental plot (CWT) of inner race defect (a) IR1 (b) IR2 (c) IR3

Table 3.4 Comparison of amplitude level and characteristic defect frequencies.

Name of fault	Simulated Results	Experimental Results
OR1	$(BPFO)_1$= 119 Hz Amplitude= 0.679m/s^2	$(BPFO)_1$= 118.75 Hz Amplitude= 0.1555 m/s^2
OR2	$(BPFO)_2$= 118.6 Hz Amplitude= 0.7844 m/s^2	$(BPFO)_2$= 118.75 Hz Amplitude= 0.1638 m/s^2
OR3	$(BPFO)_3$= 118.1 Hz Amplitude= 0.8029 m/s^2	$(BPFO)_3$= 118.75 Hz Amplitude= 0.1468m/s^2
IR1	$(BPFI)_1$= 181.64 Hz Amplitude= 0.6486 m/s^2	$(BPFI)_1$= 180 Hz Amplitude= 0.02206 m/s^2
IR2	$(BPFI)_2$= 181.64 Hz Amplitude= 0.703 m/s^2	$(BPFI)_2$= 180 Hz Amplitude= 0.03381 m/s^2
IR3	$(BPFI)_3$= 180.5 Hz Amplitude= 0.83029 m/s^2	$(BPFI)_3$= 180 Hz Amplitude= 0.1033 m/s^2
Ball	(BSF)= 58.59 Hz Amplitude= 0.7074m/s^2	(BSF)= 57.5 Hz Amplitude= 0.727 m/s^2

3.4.4 Rolling-Element Fault analysis

In order to understand the vibration response caused by the faulty rolling element, a notch fault was created upon one of the rolling elements by using electric spark erosion technique. Figure 3.16 shows time domain signal for both the simulated and experimental response. Unlike time domain signals of inner race defect and outer race defect, the rolling element defect shows more excitation of resonances. The characteristic defect frequency of the rolling element (f_{bsf}) 57.438 Hz and its second harmonic is very well observed in a FFT spectrum shown in Figure 3.17, for both simulated and experimental result. The FFT results are in very well agreement with both simulated and experimental response, however, simulation signal impulses are more definite and less damped. The CWT plot of the ball

defect for both simulated and experimental results are shown in Figure 3.18. Time interval between successive amplitudes in the band of high - frequency determines the presence of ball defect. The time interval T=0.01800 sec of simulated CWT and T=0.001800 sec of experimental CWT corresponds to the ball defect frequency. Both the time intervals of simulated and experimental CWT are in well agreement to each other. This indicates that CWT technique clearly determines the presence of ball fault.

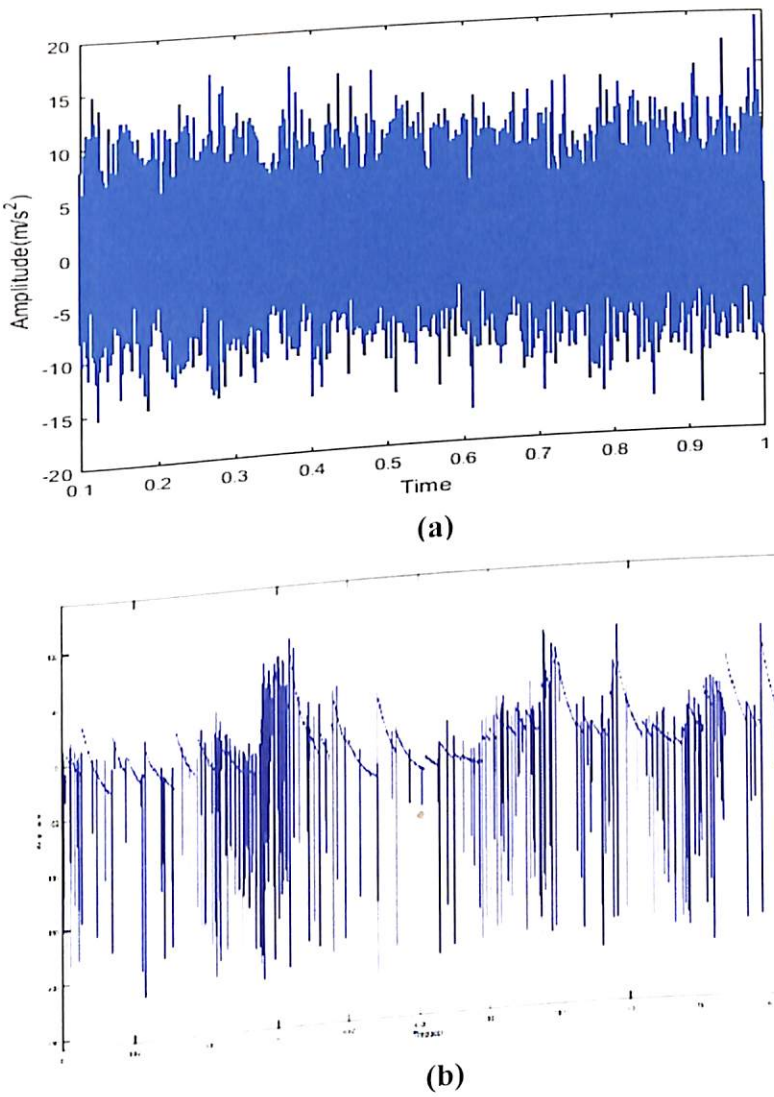

(a)

(b)

Figure 3.16 (a) Simulated and **(b)** Experimental time domain plot of ball defect.

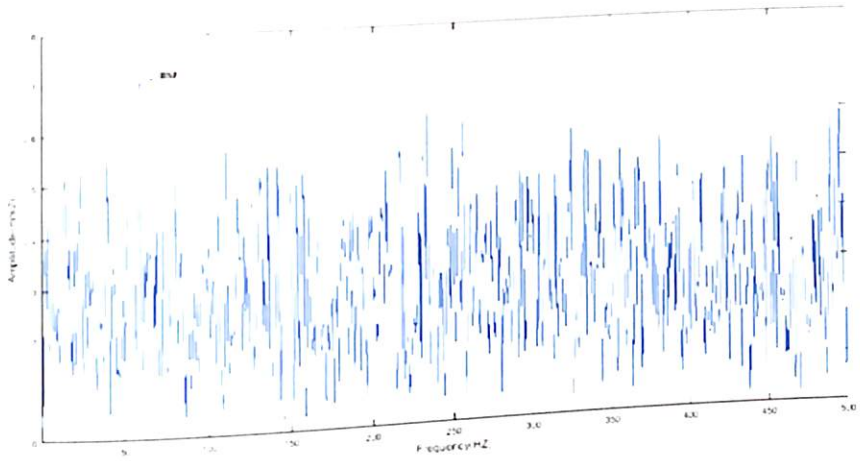

(a)

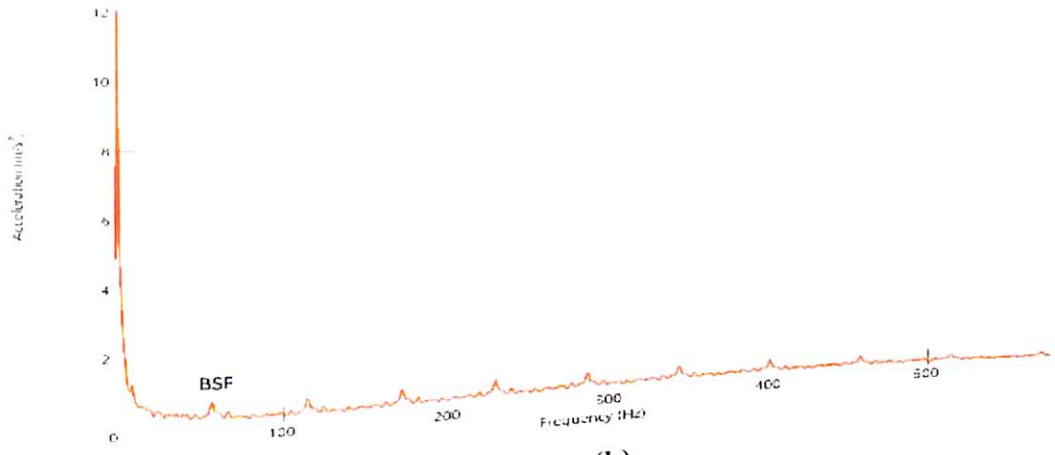

(b)

Figure 3.17 (a) Simulated and **(b)** Experimental FFT of ball defect.

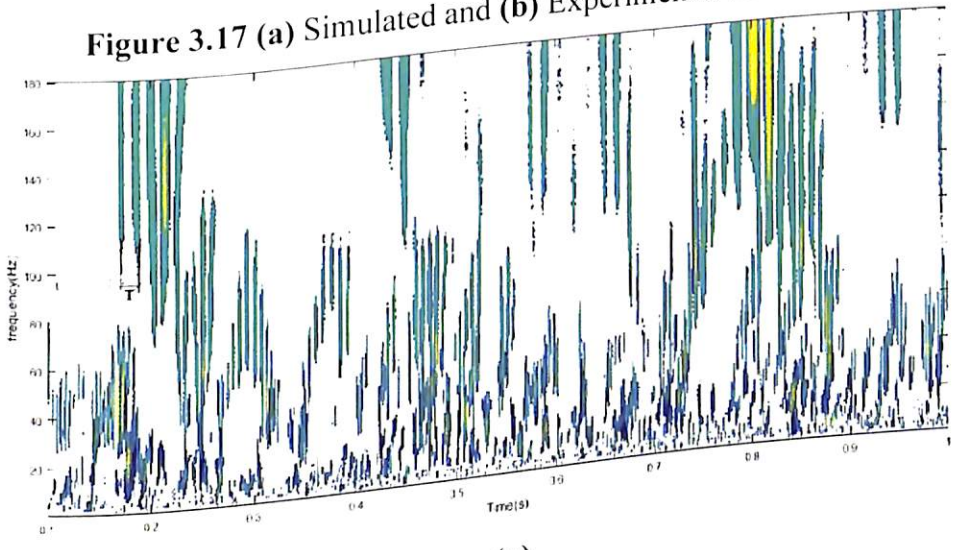

(a)

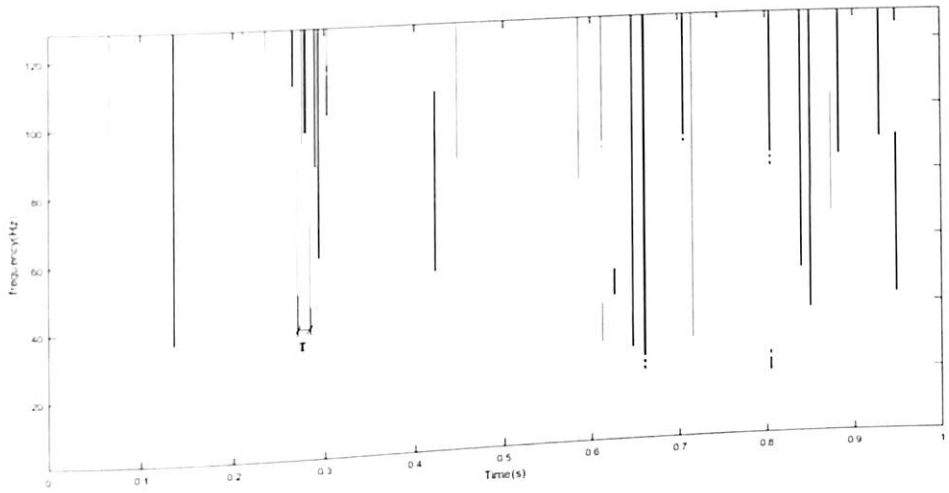

(b)

Figure 3.18 (a) Simulated and **(b)** Experimental CWT plot of Ball Defect.

3.5. Conclusion

A non-linear dynamic model is established using six-degrees of freedom to obtain the vibration response due to the localized defect. The dynamic model is used for simulating the vibration response of bearing structure due to the different sizes of defects at constant rotational speed of the shaft. The model is highly relevant in understanding the fault severity due to outer race and inner race defect of rolling element bearing upon the rotor bearing system. The model is validated with experimentation for different fault conditions. The results of the simulation and experimentation are mainly analyzed using CWT. The CWT technique potentially detects the fault by providing the time interval between consecutive amplitudes corresponding to fault frequency. It is very well observed that the simulated results are in well agreement with experimentation results and fault severity of the rolling element bearing is realized with the help of results. This chapter mainly provides the basis to understand the fault severity of the rolling element bearing. However, further research is required for understanding the fault severity of rolling element upon rotor dynamic system.

It is difficult to understand the interaction between load, speed and defect severity with the help of technique presented in this chapter. Hence chapter 4 throws light upon interaction effect of these three essential parameters.

References

1] S. Sassi, B.Badri, M.Thomas, (2007). A numerical model to predict damaged bearing vibrations, Journal of Vibration and Control 13(11) 1603–1628.

2] J. Sopanen, A.Mikkola, (2003). Dynamic model of a deep-groove ball bearing including localized and distributed defects. Part1: theory, Proceedings of the Institution of Mechanical Engineers, PartK:Journal of Multi-Body Dynamics 217(3) 201–211.

3] J. Sopanen, A.Mikkola, (2003). Dynamic model of a deep-groove ball bearing including localized and distributed defects. Part2: implementation and results, Proceedings of the Institution of Mechanical Engineers, PartK: Journal of Multi-Body Dynamics 217(3) 213–223.

4] M.Tadina, M.Bolte,V.Z.Ar, (2011). Improved model of a ball bearing for the simulation of vibration signals due to faults during run-up, Journal of Sound and Vibration 330 (17) 4287–4301.

5] D. Petersen, C.Howard, N.Sawalhi, A.M.Ahmadi, S.Singh, (2015). Analysis of bearing stiffness variations, contact forces and vibrations in radially loaded double row rolling element bearings with raceway defects, Mechanical Systems and Signal Processing 50 139–160.

6] A.M.Ahmadi, D.Petersen, C.Howard, (2015). A nonlinear dynamic vibration model of defective bearings–The importance of modelling the finite size of rolling elements, Mechanical Systems and Signal Processing 52 309–326.

7] Z. Kiral, H.Karagulle, (2003) Simulation and analysis of vibration signals generated by rolling element bearing with defects, Tribology International 36 667–678.

8] J.Urbanek, J.Antoni,T.Barszcz, (2012). Detection of signal component modulations using modulation intensity distribution, Mechanical Systems and Signal Processing 28 399–413.

9] B. Li, X.F.Chen, (2014). Wavelet-based numerical analysis: a review and classification, Finite Elem.Anal.Des.8114–31.

10] N. Sawalhi, R.B.Randall, (2008). Simulating gear and bearing interactions in the presence of faults:partI.The combined gear bearing dynamic model and the simulation of localized bearing faults, Mechanical Systems and Signal Processing 22 (8) 1924–1951.

11] Randall R.B., Sawalhi N. (2011). Signal Processing Tools for Tracking the Size of a Spall in a Rolling Element Bearing. IUTAM Symposium on Emerging Trends in Rotor Dynamics. IUTAM Book series, Vol 1011. Springer, Dordrecht.

12] H. Hong, M.Liang, (2009) .Fault severity assessment for rolling element bearings using the Lempel–Ziv complexity and continuous wavelet transform, Journal of Sound and Vibration 320 (1) 452–468.

13] Harris.T. A,1991, Rolling Bearing Analysis, Wiley-Interscience, USA.